Journal of
Synchrotron Radiation

ISSN 0909-0495

Received 13 February 2009
Accepted 29 September 2009

Analysis of tapered front-coupling X-ray waveguides

Inna Bukreeva,[a,b]* Daniele Pelliccia,[c]‡ Alessia Cedola,[a] Fernando Scarinci,[a] Mihaela Ilie,[a] Cinzia Giannini,[d] Liberato De Caro[d] and Stefano Lagomarsino[a]

[a]Istituto di Fotonica e Nanotecnologie, CNR, Via Cineto Romano 42, 00156 Roma, Italy, [b]Russian Academy of Science, PN Lebedev Physics Institute, Leninsky pr. 53, 119991 Moscow, Russia, [c]Institut für Synchrotronstrahlung, ANKA, Forschungszentrum Karlsruhe, Herman-von-Helmholtz-Platz 1, D-76344 Eggenstein-Leopoldshafen, Germany, and [d]Istituto di Cristallografia, CNR, Via Amendola 122/O, 70126 Bari, Italy. E-mail: inna.bukreeva@ifn.cnr.it

The coupling and propagation of electromagnetic waves through planar X-ray waveguides (WG) with vacuum gap and Si claddings are analyzed in detail, starting from the source and ending at the detector. The general case of linearly tapered WGs (*i.e.* with the entrance aperture different from the exit one) is considered. Different kinds of sources, *i.e.* synchrotron radiation and laboratory desk-top sources, have been considered, with the former providing a fully coherent incoming beam and the latter partially coherent beams. It is demonstrated that useful information about the parameters of the WG can be derived, comparing experimental results with computer simulation based on analytical solutions of the Helmholtz equation which take into account the amplitude and phase matching between the standing waves created in front of the WG, and the resonance modes propagating into the WG.

Keywords: X-ray waveguides; coherent X-rays; X-ray standing waves; X-ray optics.

1. Introduction

Among different X-ray optics, X-ray waveguides (WGs) have shown interesting characteristics in the production and applications of coherent X-ray nanobeams. A WG can be schematized as a very narrow channel (typical size of tens to hundreds of nanometres) in which the incoming radiation is trapped, as in an optical resonator. The beam propagates in the channel through resonant modes, and the outcoming beam, diffracted at the exit slit of the WG, can be exploited for high-resolution X-ray microscopy and microdiffraction imaging (Lagomarsino *et al.*, 1997; Di Fonzo *et al.*, 2000) and recently in coherent X-ray diffraction imaging (CXDI) experiments (De Caro *et al.*, 2007, 2008). For X-ray microscopy, the nanosized channel is used as a secondary source to magnify an object onto a detector screen, with an attainable resolution limited only by the actual size of the WG channel. On the other hand, with the CXDI technique (Miao *et al.*, 2002), resolution increase has been demonstrated, in principle bounded only by the fundamental diffraction limit. In fact, if an object is illuminated with coherent X-rays, its transmission function (projected complex refraction index) in real space can be retrieved from measurement of the diffraction pattern. Phase-retrieval techniques are used, playing the role of 'virtual' objective lenses, removing the limitation of a finite numerical aperture of real optical systems. A key point for such a technique is knowledge of the illumination function. In this regard, WGs provide a curved coherent wavefront that can be, in principle, analytically predicted, thus increasing the capabilities of phase-retrieval algorithms (Quiney *et al.*, 2005; De Caro *et al.*, 2007). It has also been demonstrated that with laboratory sources a WG can give detectable signals useful for carrying out phase-contrast imaging experiments with a spatial resolution of a few hundreds of nanometres (Pelliccia *et al.*, 2010). WGs have properties that make them worthy of further development and studies: (i) they work over a large energy range, from soft to hard X-rays; (ii) unlike capillaries, which are made of glass, WGs can have different cladding materials that can be optimized for the required energy; (iii) the roughness of the reflecting surfaces can be controlled down to fractions of a nanometre; (iv) WGs can provide beam dimensions from micrometres down to a few nanometres; (v) they are easy to fabricate, especially with the procedure that we have developed at our institute, and quite cheap; (vi) they inherently provide coherent beams, because they are based on the propagation of resonance modes; (vii) multiple WGs can be fabricated close to each other, in order to create interference patterns (Ollinger *et al.*, 2005), and (viii) WGs can be split to provide holographic devices (Fuhse *et al.*, 2006). In a general case, WGs are tapered, *i.e.* the WG gap at the exit is different (either larger or smaller) than at the entrance. Tapered WGs with a narrowing guiding layer can concentrate

‡ Present address: School of Physics, Monash University, Clayton, Victoria 3800, Australia.

beam to a very small focal spot (theoretically FWHM $\simeq$ 10 nm; Bergemann *et al.*, 2003). Optimization of the shape of the WG can give significant flux enhancement at the output end (Panknin *et al.*, 2008). During fabrication, some tools can be used to control the WG surface (scanning electron microscopy, atomic force microscopy), but the best way to characterize WG properties is with direct X-ray measurements. It is therefore important to develop a tool able to analyze the experimental results and provide feedback about the WG structure. The present work aims at a comprehensive description of the beam propagating in a linearly tapered waveguide, under different tapering conditions, and with different illuminating sources (synchrotron radiation large-scale facilities and laboratory source). On the basis of this theoretical analysis, a computer code has been developed, which provides a fast and simple comparison of the experimental results. Simple equations also provide a way to roughly estimate the essential parameters of the WG under examination without computer simulations: *i.e.* the gap and angle of tapering.

This paper is organized as follows: the basic equations of electromagnetic modes in a front-coupling (FC) planar WG are set up in §2; the theoretical analysis of electromagnetic field propagation in tapered WGs is carried out in §3; experimental results and comparison with theoretical expectations are described in §4 for different synchrotron radiation facilities and for a laboratory source; conclusions are reported in §5.

2. Front-coupling waveguide: basic equations

The guiding layer of the WG is formed by a vacuum gap d limited by two plain cladding flat surfaces of width W much larger than the gap d. This reduces the problem to one dimension. The incoming radiation is directly side-coupled into the channel (Fig. 1) with a preliminary reflection at the very entrance. In this geometry the beam, pre-reflected from the bottom plate of the WG, gives rise to standing waves just in front of the WG entrance aperture and a particular single mode can be selected at one of the resonance angles (Pelliccia *et al.*, 2007). Moreover, the effective entrance aperture and therefore the coupled power can be increased by a factor of two, owing to the pre-reflection. Unlike the FC scheme with pre- and post-reflections from the plate at the terminal parts of the WG used by Zwanenburg *et al.* (1999), we excluded post-reflection and assumed the same cladding layer termination position at the exit. This allows us to avoid an increase of the effective aperture of the WG at the exit; with our model the gap is simply d.

The propagation of electromagnetic radiation through a tapered WG is given by the solution of the Helmholtz equation,

$$\nabla^2 U(r, \varphi) + n^2 k^2 U(r, \varphi) = 0, \qquad (1)$$

where $k = 2\pi/\lambda$ is the wavevector, λ is the wavelength of the incoming X-ray radiation, $n = 1 - \delta + i\beta$ is the index of refraction of the cladding material (for vacuum or air $n = 1$)

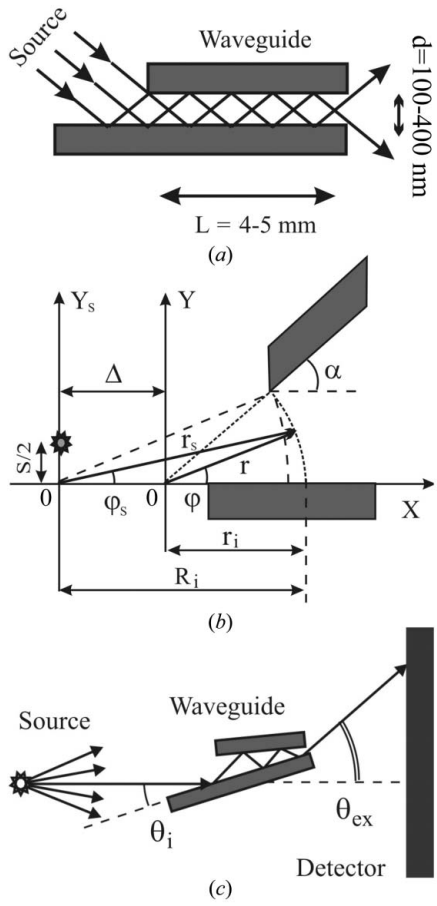

Figure 1
Scheme of a front-coupling WG with pre-reflection; (*a*) constant-gap WG; (*b*) tapered WG with polar systems of coordinates (r,φ) and (r_S, φ_S) used for analytical calculation; (*c*) schematic drawing indicating incidence θ_i and exit θ_{ex} angles.

and $U(r,\varphi)$ is the scalar wavefield satisfying the boundary conditions

$$U(\varphi = 0, \varphi = \alpha) = 0 \qquad (2)$$

at the interface vacuum gap and claddings, where (r,φ) are polar coordinates and α is the angle of tapering (see Fig. 1*b*). We exclude any penetration of the field in the cladding material. This approximation can be used when the depth of penetration, $\rho = 1/k(\theta_c^2 - \theta^2)^{1/2}$, of the field in the cladding material is much less then the gap width d ($d \gg \rho$). In the previous expression, θ is the grazing-incidence angle of the radiation and $\theta_c = (2\delta)^{1/2}$ is the critical angle of reflection for the given radiation wavelength and material. As an example, the penetration of X-rays at $\lambda \simeq 0.1$ nm for small angle $\theta < \theta_c$ is some nanometres and for a vacuum gap $d \geq 200$ nm the contribution of the evanescent field to the propagation of X-ray radiation in the WG can be neglected to a first approximation. For large angles $\theta \simeq \theta_c$ and narrower vacuum gap $d \simeq d_c = \lambda/(2\theta_c)$ [d_c is the critical gap width supporting only one mode (Bergemann *et al.*, 2003)], the penetration of radiation into the cladding layers has to be taken into account.

The general solution of the Helmholtz equation, (1), can be written as a linear combination of guided modes (eigenmodes)

of the WG, indicated by $\Psi_m(r,\varphi)$, where $m = 1, 2, \ldots, m_{\max}$ is the number of modes supported by the WG with $m_{\max} = d/d_c$,

$$U(r, \varphi) = \sum_{m=1}^{m_{\max}} c_m \Psi_m(r, \varphi). \quad (3)$$

The coefficients c_m of the combination are given by

$$c_m = \frac{1}{\|\Psi_m\|^2} \int U(r, \varphi)\, \Psi_m^*(r, \varphi)\, \mathrm{d}\varphi. \quad (4)$$

The particular solution with zero boundary condition $U(\varphi = 0, \varphi = \alpha) = 0$ can be found elsewhere (Zwanenburg *et al.*, 2000), and the expression for the mth eigenmode of the hollow WG is written as

$$\Psi_m(r, \varphi) = H^{(1)}_{m\pi/\alpha}(kr)\, \sin\left(\frac{m\pi\varphi}{\alpha}\right), \quad (5)$$

where $H^{(1)}_\nu$ is the Hankel function of the first kind. In parabolic approximation, equation (5) can be replaced by (Abramowitz & Stegun, 1965)

$$\Psi_m(r, \varphi) = \left(\frac{2}{\pi kr}\right)^{1/2} \sin\left(\frac{m\pi\varphi}{\alpha}\right) \times \exp\left[i\left(kr - \frac{m\pi^2}{2\alpha} - \frac{\pi}{4} + \frac{m^2\pi^2}{2\alpha^2 kr}\right)\right]. \quad (6)$$

3. Field propagation

The propagation of the electromagnetic field inside a tapered waveguide has been theoretically analyzed by computer simulations based on the numerical solution of the analytical equations reported above. The computer simulations allow different set-ups and waveguide layouts to be considered, for which the equations cannot be solved analytically. The propagation problem has been accounted for by modelling a suitable X-ray source, propagating the field to the WG entrance, modelling the coupling between the incoming field and the waveguide eigenmodes, then following the electromagnetic propagation inside the channel, and finally in free space to the detector. If synchrotron sources are used, then in general the large distance between source and WG entrance makes it possible to consider the incident waves as plane waves, but in the case of laboratory sources (or in the case of prefocusing optics) the plane-wave approximation cannot be used, and the physical size of the source must be taken into account. The computer code, as described in the present chapter, can be applied to any linearly tapered WG with the approximation of negligible roughness of the cladding surfaces and low absorption losses owing to the reflections.

3.1. From source to WG

In the computer code[1] a laboratory X-ray source is modelled by a set of elementary spherical radiators with the initial phase randomly distributed within the interval $[-\pi, \pi]$. The wave from an elementary radiator after reflection in front of the entrance aperture of the WG gives rise to standing waves that, inside the guiding layer, can be written as a linear combination of modes [equation (3)]. The distribution of intensity for an extended laboratory source is then found as a sum of contributions from independent radiators. The spectrum of the radiation from the X-ray tube ($K_\alpha + K_\beta$ lines for the copper target, $E \simeq 8$ keV) including the continuous wide Bremsstrahlung spectrum from 3 to 30 keV is taken into account in the computer code.

Let us consider, for example, an X-ray point source located at a distance $S/2$ from the axis 0–X illuminating a WG in asymmetric (*i.e.* with a pre-reflection) geometry (Fig. 1*b*). For convenience we introduce a new polar coordinate system (r_S, φ_S) with the pole at the intersection between the axis 0–X and the perpendicular to this plane from the source radiator (Fig. 1*b*). Standing waves are formed in front of the WG entrance aperture (Fig. 2*a*). The standing-wave pattern can be considered as the interference between the real source and an image source located at $-S/2$ with respect to the reflecting plane, emitting with a dephasing equal to π with respect to the real one. Nodal lines (*i.e.* loci of minimum of intensity in Fig. 2*a*) for the interference pattern produced by two point sources are hyperbolas in the general case. Taking into account the phase shift π between the emitted waves, the hyperbolas satisfy the equation, in polar coordinates, $n\lambda =$

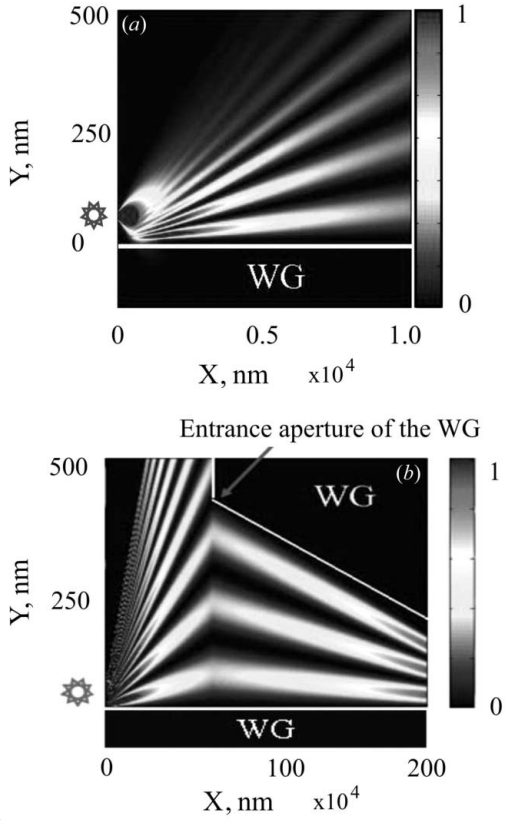

Figure 2
(*a*) Standing waves in front of the entrance aperture of the WG; (*b*) phase mismatch at the entrance aperture of the WG (illustration not to scale).

[1] Supplementary data for this paper are available from the IUCr electronic archives (Reference: IE5030). Services for accessing these data are described at the back of the journal.

$S\sin\varphi_S$, where S is the distance between the real and the image source. At distances much greater than the wavelength, the nodal lines appear as straight radial lines that in the small-angle approximation can be written as $\varphi_S = y/x \simeq n\lambda/S$.

The standing wavefield is a solution of the Helmholtz equation, (1), in the coordinate system (r_S, φ_S) of the point source (see Fig. 1*b*) with boundary conditions $U(\varphi_S = n\lambda/S) = 0$,

$$U(r_S, \varphi_S) = H^{(1)}_{k\theta_i R_i}(kr_s)\sin\left(k\theta_i R_i \varphi_S\right), \tag{7}$$

where $\theta_i = S/(2R_i)$ is the grazing-incidence angle and R_i is the distance of the WG from the source and the entrance aperture (Fig. 1*b*).

3.2. Coupling between the incoming field and the resonance modes

The incoming field [equation (7)] excites a set of modes in the guiding layer and it can be expanded in the series of eigenmodes of the WG. Taking into account equation (5), the coefficients of expansion (4) can be written in the parabolic approximation as

$$c_m \simeq \frac{H^{(2)}_{m\pi/\alpha}(kr_i)\, H^{(1)}_{k\theta_i R_i}(kR_i)}{\left\|\Psi_m\right\|^2} \times \int_0^{\alpha} \sin\left(\frac{m\pi\varphi}{\alpha}\right)\sin(kr_i\theta_i\varphi)\,\exp\left(\pm ik\Delta\frac{r_i}{R_i}\frac{\varphi^2}{2}\right)\mathrm{d}\varphi, \tag{8}$$

where Δ is the distance between the origins (poles) of the two coordinate systems, respectively, of the source and of the WG (see Fig. 1*b*). The choice of the sign in (8) depends on the relative position of the poles. $|\Psi_m| = \alpha/(\pi\kappa r_i)$ is the norm of the eigenmode Ψ_m.

The optimal matching of the incoming field with the vacuum gap takes place and a single mode Ψ_m can be excited when the arguments of the sine functions in the integral (8) are equal: $m\pi\varphi/\alpha = kr_i\theta_i$. From this relation the resonance angles are given by

$$\theta_m = \frac{m\pi}{kr_i\alpha}, \qquad m = 1, 2, 3, \ldots. \tag{9}$$

Taking into account that at the entrance aperture of the WG the gap is equal to $d = r_i\alpha$, equation (9) is equivalent to the well known resonance condition

$$\theta_m = m\lambda/2d. \tag{10}$$

In the general case, the wavefront curvatures of the incident wave and of eigenmodes at the entrance aperture of the WG are different (Figs. 1*b* and 2*b*). Therefore even at resonance conditions the phase mismatch at the entrance can excite more than one mode (Bergemann *et al.*, 2003). Strong coupling of the incident beam into the particular single mode $\Psi_m(r,\varphi)$ can be provided only for small phase parameter $\xi = [k\Delta\alpha^2 r_i/(\pi R_i)]^{1/2} \leq 1$, which gives a condition on the tapering angle α for single mode excitation,

$$\left|\alpha \pm \beta\right| \leq \lambda/2d, \tag{11}$$

where $\beta = d/R_i$ is the WG numerical aperture. The plus sign holds for converging WGs and the minus sign for diverging ones.

If the resonance conditions (9) or the inequality (11) are not satisfied, all modes are contextually excited in the guiding layer and the field profile in the WG is given by (3) with coefficients given by (8).

3.3. Mode propagation inside the WG

The analysis performed so far started from the solution of the Helmholtz equation, (1), with zero field at the boundaries, (2). Therefore the energy losses owing to reflection are neglected. This does not correspond to the real situation. In the general case the propagation of modes in the guiding layer can be described accurately as a solution of (1) with boundary conditions that take into account penetration and absorption of field in the claddings, but if the depth of penetration is much less than the gap width d ($d \gg \rho$) a simplified expression for the coefficient of transmission can be used. We estimate the coefficient of transmission of mode with number m for a tapered WG as the product of Fresnel coefficients of successive reflections of the incident plane wave with resonance angle θ_m [see equation (10)],

$$R_m \simeq \prod_{n=1}^{N} R_{\mathrm{fr}}(\theta_m \pm n\alpha), \tag{12}$$

where N is the maximum number of reflections. For a WG without tapering ($\alpha = 0$), the coefficient of transmission is

$$R_m \simeq R^N_{\mathrm{fr}}(\theta_m) \simeq R^{L\theta_m/d}_{\mathrm{fr}}(\theta_m). \tag{13}$$

Taking into account equation (12), the total field profile is given by

$$U(r, \varphi) = \sum_{m=1}^{m_{\max}} c_m R_m \Psi_m(r, \varphi). \tag{14}$$

3.4. Propagation from the WG exit to the detector

Sufficiently far from the WG exit, the field at the detector can be calculated as the Fourier transform of the field at the exit aperture of the WG, given by (14). We should distinguish two different situations: the first when the incoming wave is fully coherent, and the second when the WG is illuminated by a partial coherent wave.

3.4.1. Coherent plane wave. Some examples of calculated patterns for the constant-gap and tapered WGs are shown in Fig. 3, considering an incoming plane wave and a WG with vacuum gap and Si claddings. The intensity distribution $I(\theta_i, \theta_{\mathrm{ex}})$ is presented in the coordinate system where the abscissa θ_i is the grazing-incidence angle of the incoming beam and the ordinate θ_{ex} is the exit angle of radiation at the terminal part of the WG (in θ–2θ geometry) (see Fig. 1*c*). Each picture is a composite where the distribution of intensity along θ_{ex} is presented as a function of the incidence angle θ_i. One can see a swallow-tail-like distribution with bright spots arranged along two lines

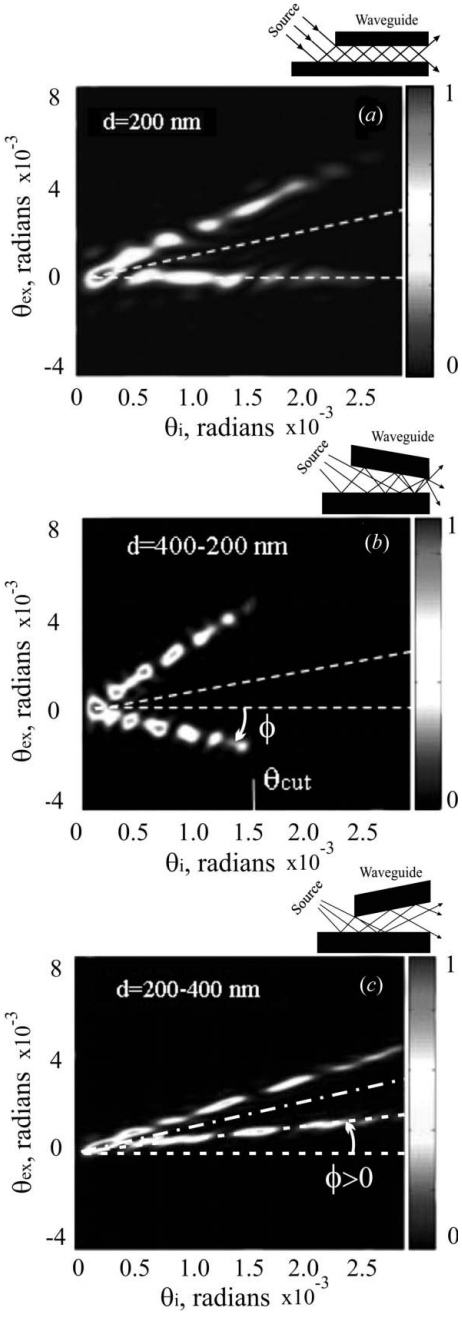

Figure 3
Diffraction pattern from the vacuum-gap Si WG with constant-gap (*a*), converging (*b*) and diverging (*c*) waveguides. The length of the WGs is L = 4 mm. A plane wave with wavelength λ = 0.154 nm forms standing waves in front of the entrance aperture of the WG.

$$\theta_{ex} = \theta_i(1 \pm d_{in}/d_{ex}), \tag{15}$$

where d_{in} and d_{ex} are the gap values at the entrance and at the exit aperture of the WG, respectively. Equation (15) gives two symmetrical lines with respect to the median $\theta_{ex} = \theta_i$. For the parallel-plate waveguide ($\Omega = d_{in}/d_{ex} = 1$) the first line $\theta_{ex} = 0$ is parallel to the axis 0–θ_i and the second one $\theta_{ex} = 2\theta_i$ is tilted at an angle arctan(2) with respect to the 0–θ_i axis (Fig. 3*a*). For the convergent WG (narrowing vacuum gap, Fig. 3*b*), the parameter $\Omega > 1$, the angles between the two branches are larger than for the constant-gap WG, and the angle $\varphi = \phi$ = arctan(1 − Ω) between the first line and the axis 0–θ_i is negative (Fig. 3*b*). For the divergent WG (expanding vacuum gap, Fig. 3*c*) the angle between the two branches is smaller than for the constant-gap WG, the parameter $\Omega < 1$, and the angle ϕ = arctan(1 − Ω) is positive (Fig. 3*c*). Moreover, it should be noted that the intensity cut-off corresponds to an incidence angle $\theta_{cut} = \theta_c d_{ex}/d_{in}$ (see Fig. 3*b*) which is dependent on the shape of the device.

Therefore the experimental diffraction pattern (θ_i, θ_{ex}) gives information about the kind of tapering (narrowing or expanding vacuum gap), and together with (15) allows an estimate of the ratio α/d_{ex} (we take into account that $\Omega = 1 + L\alpha/d_{ex}$).

3.4.2. Partially coherent wave from laboratory source. All equations for a coherent incidence wave can be used for a laboratory source located far enough from the WG: $R_i \gg 2dS_0/\lambda$ (S_0 is the size of the focal spot for the table-top source). The previous expression corresponds to the condition that the coherence length of the incoming beam is larger than twice the WG gap at the entrance d_{in}. Otherwise a special code for an incoherent X-ray source must be used (see §3.1).

The intensity distribution calculated for a laboratory microsource with a spot size of 15 µm and wavelength $\lambda \simeq$ 0.154 nm is shown in Figs. 4(*a*)–4(*c*). As in the case of the plane wave, three different geometries have been considered, with no change regarding the WG parameters: (*a*) constant-gap WG; (*b*) converging WG; (*c*) diverging WG. The distance between the source and the WG was R_i = 2.5 cm, which corresponds to a coherence length of the incident wave at the WG entrance $h \simeq$ 260 nm, less than the effective entrance aperture of the guiding layer $d_{eff} = 2d_{in}$. For this case we use the computer code described in §3.1 for laboratory table-top sources.

From Fig. 4 we can see that the partial coherence of the incoming field broadens the wing of the diffraction pattern. This effect is particularly evident for the converging WG with an entrance aperture d_{in} = 400 nm, which is considerably larger than the coherence length of the incoming field. Even in this case, however, we can receive information about the kind of tapering (constant, narrowing or expanding vacuum gap) and we can approximately estimate the ratio α/d_{ex}.

4. Experimental results

The analytical treatment presented above has been compared with a number of experimental results taken with both laboratory and different synchrotron radiation sources. WGs were fabricated with Si slabs, using lithographic processes and wafer bonding. The WGs had an entrance aperture gap (d) × width (w) of hundreds of nanometres (d) × a few millimetres (w), and a length L of about 4–5 mm (see Fig. 1*a*). The examples reported here provide an overview of different situations, to validate the theoretical model. Therefore we will present both very nice patterns indicating quite perfect WGs, and patterns with very high values of the tapering angle.

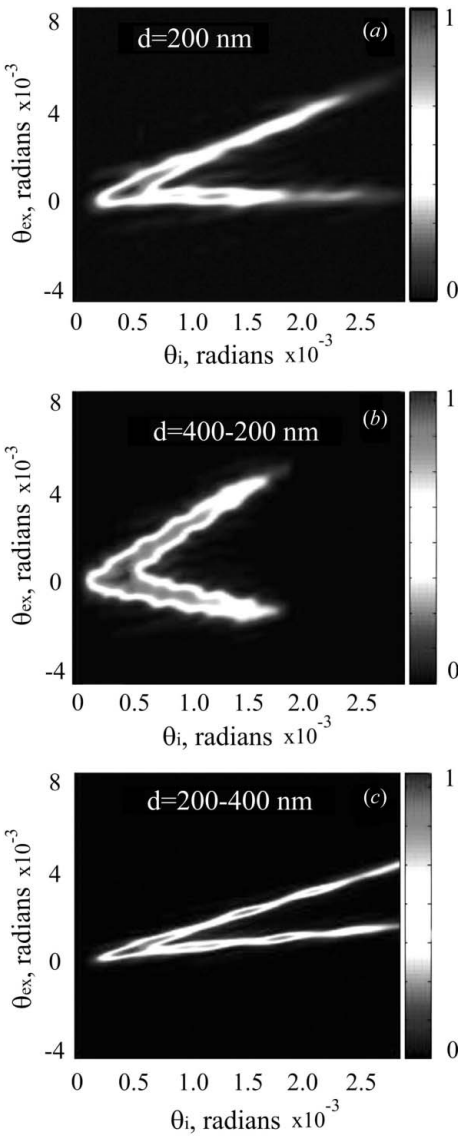

Figure 4
Diffraction pattern from the exit aperture of the WG with Si claddings and vacuum guiding layer for constant-gap (*a*), converging (*b*) and diverging (*c*) waveguides. Microsource spot size S = 15 µm, λ = 0.154 nm. Source–WG distance R_i = 2.5 cm.

4.1. Experimental results at synchrotron radiation facilities

Results are presented for measurements carried out at ELETTRA (Trieste), ANKA (Karlsruhe) and ESRF (Grenoble) synchrotron radiation facilities. They cover a wide range of experimental conditions. The ELETTRA results are related to a low-tapering WG, in which the different resonance modes are well separated. The results of ANKA and ESRF report strongly tapered waveguides measured in different conditions of bandwidth. The experimental pictures are composites taken from the two-dimensional images (frames) which show, for each incidence angle θ_i, the intensity distribution along the WG width (w) and the exit angle θ_{ex}. For each frame the intensity along θ_{ex} is averaged along the width w for a few pixels.

4.1.1. Experimental results at ELETTRA (Trieste, Italy). The measurements were taken at the microfluorescence beamline. The beam from the bending magnet was monochromated by a double-crystal Si (111) monochromator, dispersing in the vertical plane, and limited by slits at about 1.8 mm (H) × 0.2 mm (V) before the WG.

The WG was aligned with its reflecting surfaces close to the horizontal plane. A motorized support with six degrees of freedom allowed for careful orientation of the waveguide with respect to the incident beam. A CCD camera with nominal pixel size of 12.3 µm and measured point spread function of about 20 µm was placed downstream of the WG. The measurements were taken at a photon energy of 7665 eV.

The distribution of intensity on the detector is shown in Fig. 5 in the previously described coordinate system (θ_i,θ_{ex}) where the abscissa reports the incidence angle and the ordinate the exit angle in the laboratory frame. The experimental diffraction pattern (Fig. 5*a*) is compared with the computer calculation for the silicon WG with a vacuum gap of 430 nm

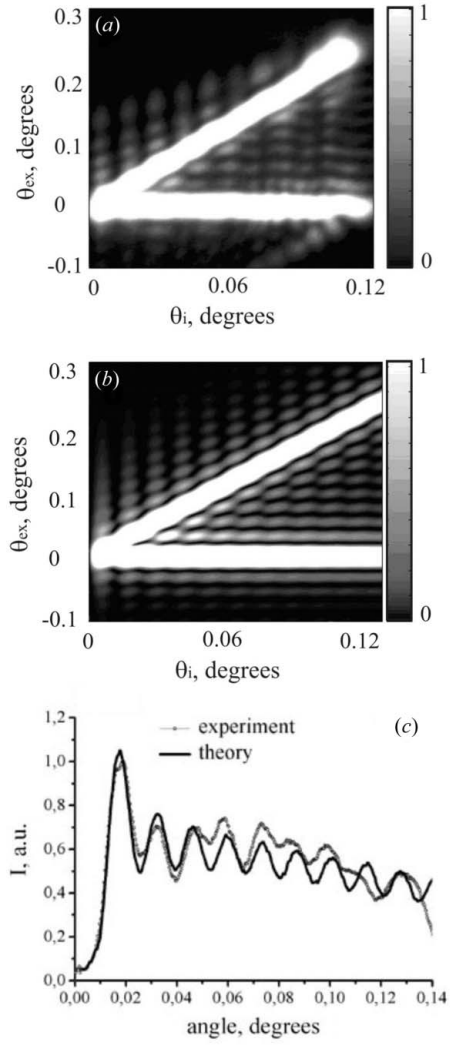

Figure 5
Diffraction pattern on the detector as a function of incidence θ_i and exit θ_{ex} angles (λ = 0.161 nm); (*a*) experimental result; (*b*) computer code; (*c*) distribution of intensity along the axis 0–θ_i for experimental (dotted line) and computer (full line) data. WG length L = 4.6 mm, gap d = 430 nm.

(Fig. 5*b*). Clear modal structure is seen on both the experimental and the theoretical distributions. The diffraction patterns consist of separated bright spots corresponding to independent modes located along two lines, equation (15). The first line is parallel to the axis 0–θ_i and the second one is tilted at an angle arctan(2), in agreement with the theory for the constant-gap WG. In between these lines secondary maxima are clearly seen, indicating good coherence of the exit beam. In Fig. 5(*c*) we report the intensity distribution along the axis 0–θ_i for both the experimental (dotted line) and theoretical (full line) distributions.

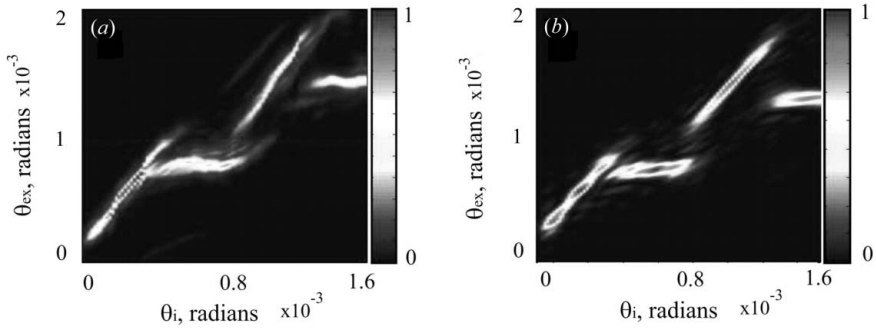

Figure 6
(*a*) Experimental results at ANKA; (*b*) computer simulation for a diverging tapered WG with a gap of 360 nm at the entrance and 1600 nm at the exit.

4.1.2. Experimental results at ANKA (Karlsruhe, Germany). WGs were also tested at the beamline Fluo at ANKA. We used for all measurements the energy $E = 11$ keV, selected by double-multilayer monochromator with bandwidth $\Delta E/E \simeq 10^{-2}$. No additional optics was used. The CCD detector with effective pixel size of 1 μm was located at a distance of 15 cm from the exit aperture of the WG.

The distribution of intensity on the detector for different pairs of incidence θ_i and exit θ_{ex} angles is shown in Fig. 6. In the figure, part (*a*) refers to experimental diffraction patterns, and part (*b*) to computer simulations. In this case the diffraction pattern is more complex, and no discrete modal structure is visible, owing also to larger values of gap and to quite relevant tapering angle. In any case, the computer simulations help to determine the WG parameters.

4.1.3. Experimental results at ESRF (Grenoble, France). Experiments were performed at the ID1 beamline of the European Synchrotron Radiation Facility (ESRF) in Grenoble, using photons of 11 keV (λ = 0.1127 nm), monochromated by a Si(111) double crystal. A CCD camera with nominal pixel size of 2 μm was put at a distance 0.6 m from the WG. The results presented here refer to tapered waveguides with a large angle of tapering ($\alpha \simeq 2 \times 10^{-4}$ rad). The experimental results with the related computer simulations are shown in Figs. 7(*a*) and 7(*b*), respectively. The WG shown in Fig. 7 is measured in the θ–2θ geometry with the detector fixed. From the computer simulations it appears that the measured waveguide is diverging, with entrance and exit gap values of d_{in} = 150 nm and d_{ex} = 670 nm, respectively. A good agreement is found between experimental results and computer simulations.

4.2. Experimental results with a laboratory X-ray microsource

A set of measurements for the tapered WGs was also carried out with a laboratory source. A conventional source with nominal size of 15 μm and Cu target (Cu $K\alpha$, λ = 0.154 nm, bandwidth $\Delta\lambda/\lambda \simeq 10^{-3}$) was used. The WGs were put at a distance of 3 cm from the source. A 30 μm slit was placed in front of the WG entrance to limit background. The far-field intensity distribution was measured using the CCD camera with a pixel size of 12.3 μm at a distance of 41 cm downstream from the WG exit. The experimental diffraction patterns, together with the corresponding computer simulations, are shown in Figs. 8(*a*)–8(*d*). Figs. 8(*a*) (experimental) and 8(*b*) (simulated) show the results for a 4.5 mm-long diverging tapered WG, with the vacuum gap expanding from 150 nm to 330 nm with an angle of 4×10^{-5} rad. Figs. 8(*c*) (experimental) and 8(*d*) (simulated) show the intensity distribution for a 4.9 mm-long WG with the gap narrowing from 305 nm to 200 nm. The coherence length of the table-top microsource at the entrance of the WG is h = 300 nm. Comparing this value with the double aperture of the WG, $2d_{in}$ = 300 nm, shown in Figs. 8(*a*) and 8(*b*), it is possible to conclude that in this case the source is totally coherent for the WG. For the WG shown in Figs. 8(*c*) and 8(*d*), the coherence length of the X-ray radiation, h = 300 nm, is less than the double aperture of the WG, $2d_{in}$ = 610 nm, and broadening of the diffraction pattern owing to the finite size of the source takes place. In both cases, from the position of the wings in the diffraction pattern, we can easy receive information about the sign of tapering of the WG (diverging or converging), and from the angle between the wings we can estimate the tapering angle.

In the computer simulation the X-ray spectrum of the Cu target including the K lines and the white Bremsstrahlung is

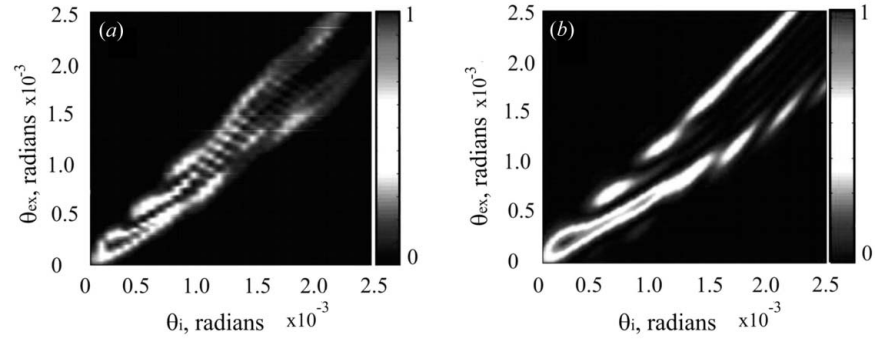

Figure 7
(*a*) Experimental results at ESRF; (*b*) computer simulation for a diverging tapered WG with gap d = 150 nm at the entrance and d = 670 nm at the exit.

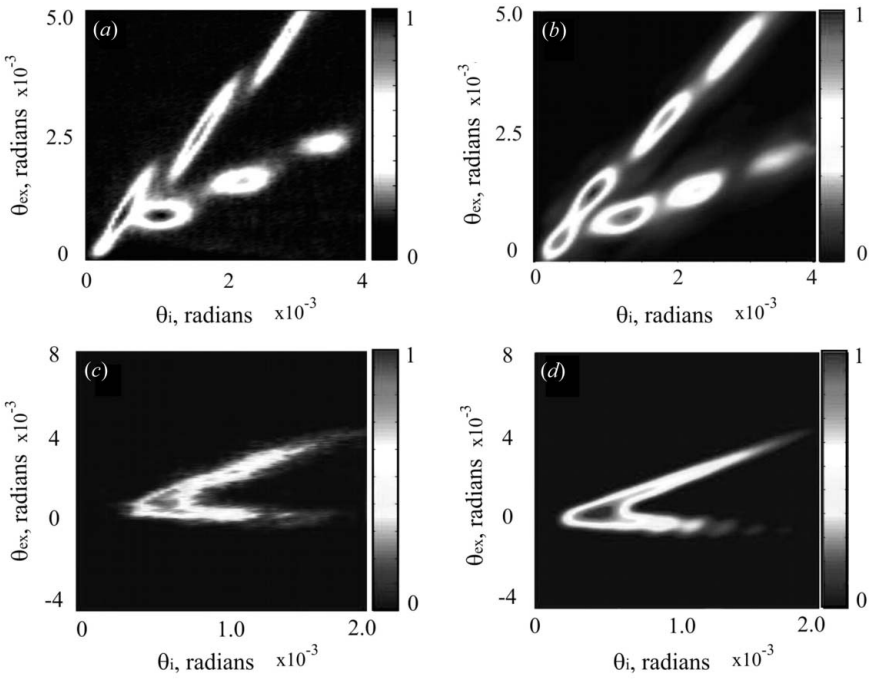

Figure 8
Far-field diffraction patterns at the detector for the table-top source (λ = 0.154 nm); (a,c) experimental results; (b,d) computer simulations. From the computer simulations it results that the WG in (a) and (b) has a length of 4.5 mm, a tapering angle $\alpha = 4 \times 10^{-5}$ rad, a gap at the entrance d_{in} = 150 nm and a gap at the exit d_{ex} = 330 nm. The WG shown in (c) and (d) has a length L = 4.9 mm, a tapering angle $\alpha = -2.2 \times 10^{-5}$ rad, d_{in} = 305 nm and d_{ex} = 200 nm.

taken into account. The effect of the Bremsstrahlung can be seen in Fig. 8(b) as a weak halo around the bright spots, in good agreement with the experimental result shown in Fig. 8(a). The intensity of the halo is at the level of the background, and does not provide any additional information. In Figs. 8(c) and 8(d) the grey intensity level is set in order to exclude background, so as to have a larger dynamic range to display the relevant features in the bright spots.

5. Conclusions

A theoretical tool able to provide useful information about the propagation of the electromagnetic field in vacuum-gap planar X-ray waveguides has been presented. Both constant-gap and tapered waveguides have been taken into account, and it has been shown that computer simulation can provide the structural parameters of the WG, with good agreement with experimental results taken both with synchrotron radiation and with a laboratory microsource.

The results presented here, and the availability of a robust simulation tool, can also open the way to another possible application of X-ray WGs, *i.e.* their use as a very sensitive optical element to characterize the incident beam in both synchrotron radiation and laboratory sources.

W. Jark is very gratefully acknowledged for his precious contribution in characterization of the WG at ELETTRA. The authors are indebted to R. Simon for the experimental collaboration at the beamline Fluo at ANKA. The staff at ID1 at ESRF are also gratefully acknowledged for their help. The project SPARX and PRIN 2007ZT39FN_003 are acknowledged for partial financial support. The COST action MP6010 is also acknowledged.

References

Abramowitz, M. & Stegun, I. A. (1965). *Handbook of Mathematical Functions*, ch. 9.1–9.2. New York: Dover.
Bergemann, C., Keymeulen, H. & van der Veen, J. F. (2003). *Phys. Rev. Lett.* **91**, 204801.
De Caro, L., Giannini, C., Cedola, A., Pelliccia, D., Lagomarsino, S. & Jark, W. (2007). *Appl. Phys. Lett.* **90**, 041105.
De Caro, L., Giannini, C., Pelliccia, D., Mocuta, C., Metzger, T. H., Guagliardi, A., Cedola, A., Bukreeva, I. & Lagomarsino, S. (2008). *Phys. Rev. B*, **77**, 081408.
Di Fonzo, S., Jark, W., Lagomarsino, S., Giannini, C., De Caro, L., Cedola, A. & Muller, M. (2000). *Nature (London)*, **403**, 638–640.
Fuhse, C., Ollinger, C. & Salditt, T. (2006). *Phys. Rev. Lett.* **97**, 254801.
Lagomarsino, S., Cedola, A., Cloetens, P., Di Fonzo, S., Jark, W., Soullié, G. & Riekel, C. (1997). *Appl. Phys. Lett.* **71**, 2557–2559.
Miao, J. W., Ishikawa, T., Johnson, B., Anderson, E. H., Lai, B. & Hodgson, K. O. (2002). *Phys. Rev. Lett.* **89**, 088303.
Ollinger, C., Fuhse, C., Jarre, A. & Salditt, T. (2005). *Physica B*, **357**, 53–56.
Panknin, S., Hartmann, A. K. & Salditt, T. (2008). *Opt. Commun.* **281**, 2779–2783.
Pelliccia, D., Bukreeva, I., Ilie, M., Jark, W., Cedola, A., Scarinci, F. & Lagomarsino, S. (2007). *Spectrochim. Acta*, B**62**, 615–621.
Pelliccia, D., Cedola, A., Sorrentino, A., Bukreeva, I. & Lagomarsino, S. (2010). In preparation.
Quiney, H. M., Nugent, K. A. & Peele, A. G. (2005). *Opt. Lett.* **30**, 1638–1640.
Zwanenburg, M. J., Bongaerts, J. H. H., Peters, J. F., Riese, D. & van der Veen, J. F. (2000). *Physica B*, **283**, 285–288.
Zwanenburg, M. J., Peters, J. F., Bongaerts, J. H. H., de Vries, S. A., Abernathy, D. L. & van der Veen, J. F. (1999). *Phys. Rev. Lett.* **82**, 1696–1699.